Advances in Understanding Plasma Rotation and Ion Thermal Transport Using Main Ion Measurements in DIII-D

S.R. Haskey[1], B.A. Grierson[1], C. Chrystal[2], A. Ashourvan[1], D. J. Battaglia[1], T. Stoltzfus-Dueck[1], M. Van Zeeland[2]

[1] *Princeton Plasma Physics Laboratory, Princeton, NJ 08543, USA*

[2] *General Atomics, PO Box 85608, San Diego, CA 92186, USA*

Advances in main-ion (D+) charge exchange spectroscopy (MICER) [1, 2] have enabled direct measurements of the deuterium properties in the pedestal region on DIII-D revealing clear differences between the temperatures of D+ and the more commonly measured C6+ impurity ions approaching the separatrix. Detailed thermal transport analysis is performed for a DIII-D ITER baseline H-mode discharge using these measurements, which play an important role in the inferred ion and electron heat fluxes due to the large ion-electron collisional exchange term approaching the separatrix. The combination of MICER measurements and the radial electric field inferred using impurity CER [3] allow the components of the D+ force balance and poloidal rotation to be calculated. We find that for the ITER baseline case the thermal transport is approximately at the neoclassical level outside the pedestal top, while the D+ poloidal rotation is significantly larger than predicted by local neoclassical theory.

Temperature profiles in the pedestal region for the D+, C6+, and electrons for a DIII-D ITER baseline shot following the L-H transition and just before the first ELM are shown in Figure 1. A correction for the Zeeman and fine structure effects [4] on the observed temperatures has been included leading to a reduction of the C6+ temperature by approximately 65eV at the edge for these conditions and having negligible effect on the D+ measurement. There is some uncertainty in the exact magnitude of this correction due to the assumption of statistically populated upper levels. Inside the top of the pedestal (ρ<0.94, ρ=sqrt(normalized

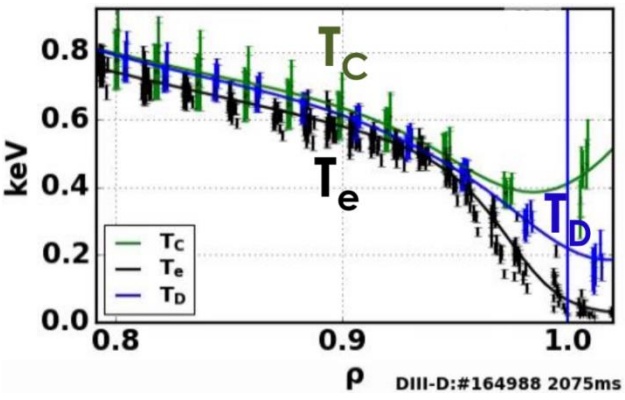

Figure 1: The electron, main-ion and impurity ion temperatures. Both ion temperatures have been corrected for Zeeman and fine structure broadening.

toroidal flux)) this correction brings the temperatures of the two ion species into close agreement (compare with Fig. 5b in [5] which does not have this correction applied). This is expected based on the rapid equilibration time between the two species (10s of microseconds) compared with the radial transport time scale (~ms). However, contrary to expectations, for $\rho>0.94$ the impurity temperature diverges from the D+ and e- values, and in some cases starts increasing very near or outside the separatrix. This type of behavior is commonly seen in these profiles on DIII-D.

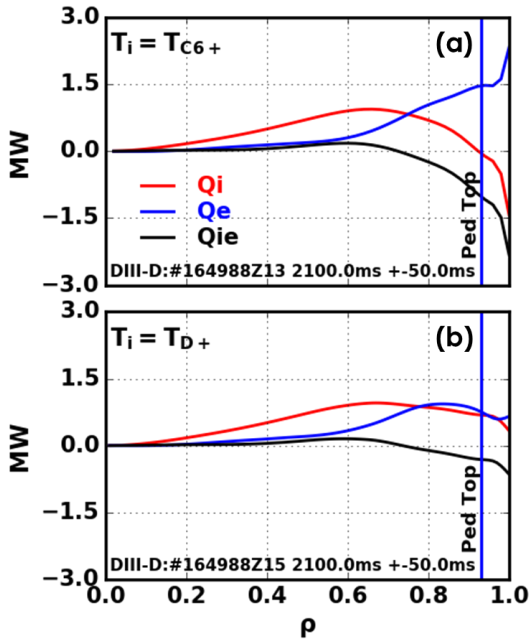

Figure 2: Volume integrated ion and electron heat fluxes, and the ion-electron collisional exchange term using the impurity temperature (a) and main ion temperature (b).

The elevated impurity ion temperatures may be due to non-local effects where the measurement is dominated by tail ions whose drift orbits take them across the pedestal region. For a 500eV Maxwell-Boltzmann distribution at the top of the pedestal, 11% of the ions will have energy greater than 1.5keV. These ions can have orbit widths covering a large portion of the pedestal and trapped ions will travel from the inside of their orbit to the outside on order 200μs for C6+. Additionally, for these tail ions the energy collision time will be significantly larger than would be expected based on the local thermal temperature due to their larger velocities. The similarity between these timescales means that these orbits can be completed without the non-local C6+ equilibrating with the D+, providing a possible explanation for the elevated impurity temperatures. Similar elevated temperatures were found using XGC0 for a QH-mode case [6]. The same argument could be made for D+; however, the main ion density gradient is typically not as sharp as the impurities, so the presence of a significant local D+ population may prevent the non-local tail ions from dominating the measurement to the same extent. This effect may contribute to the difference between the D+ and electron temperature approaching the separatrix.

In order to understand the processes responsible for driving thermal transport in the pedestal region, theory predictions must be compared with ion thermal transport calculated using the time histories of the profiles along with the sources and sinks. Figure 2 shows the volume integrated ion and electron heat fluxes and the collisional exchange term between the ions and electrons ($\sim n_e n_i (T_e - T_i)/Te^{3/2}$) as calculated by TRANSP for this discharge. When using the impurity temperature (Fig 2a) without correcting for the Zeeman effect, the exchange term becomes large near the edge due to the temperature differences and the low electron temperature. This ultimately leads to a negative ion heat flux through the pedestal region which seems implausible. However, when the same calculation is performed using the measured D+ profile (Fig 2b), a more plausible positive heat flux is calculated. The impact of the impurities on the ion thermal transport is not included here.

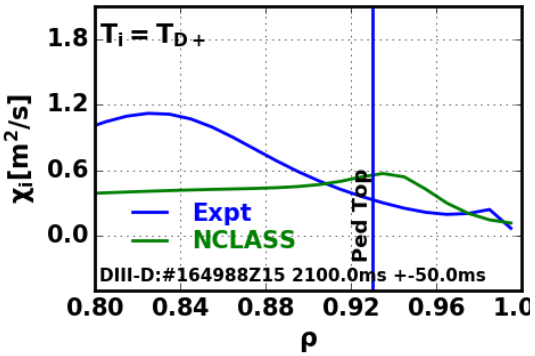

Figure 3: Comparisons between the effective thermal conductivity inferred by TRANSP using the D+ temperature measurements and predictions using the NCLASS code.

Using the calculated ion heat flux in Fig 2b, it is possible to also extract an inferred effective ion thermal diffusivity (χ_i) from TRANSP and compare the value with expectations based on neoclassical theory using the NCLASS code (Fig 3). Inside the pedestal top, the experimental diffusion is significantly larger than the neoclassical level, as expected due to turbulent transport. In the pedestal region, the transport is approximately at the neoclassical level for this case. Historical issues such as negative ion heat fluxes have meant that pedestal ion thermal transport analysis on DIII-D has been quite limited. In [7], approximately neoclassical χ_i was found in an H-mode case and in [8] reasonable agreement with ITG based transport was found early in the H-mode phase and experimental values above both ITG and neoclassical χ_i estimates later in the H-mode phase. In both cases impurity measurements were used. Detailed modeling of a QH-mode discharge using the XGC0 code also showed that the thermal transport was at the neoclassical level when extended neoclassical effects such as neutrals, non-locality, and non-Maxwellian distribution functions are included [6]. A significant amount of work has been performed on ASDEX Upgrade in this area using either impurity temperature measurements or main-ion measurements in helium plasma with the general finding that the pedestal ion thermal transport is neoclassical across a range of collisionalities [9] without having to invoke extended neoclassical transport effects.

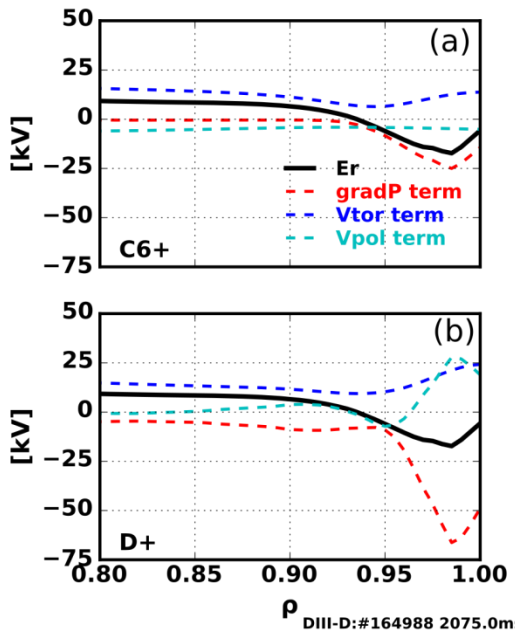

Figure 4: Components of force balance for the impurities (a) and the main ions (b)

The combination of impurity CER and MICER allows the main-ion poloidal rotation to be inferred based on force balance: $E_r=\nabla P/Zen+V\phi B\theta-V\theta B\phi$. The three terms in this equation are species dependent and are shown in Fig 4 for the C6+ impurities (a) and the main-ions (b) with the Vpol term being inferred for the D+ using Er from the impurity measurements. The D+ Vpol term peaks around 25kV/m which corresponds with a poloidal rotation of ~18km/s in the ion diamagnetic direction. This value is significantly larger than expectations based on neoclassical theory, which are typically on the order of 1-2km/s due to strong damping. Similar large main-ion poloidal rotations have been observed in DIII-D He plasmas [10] but not on ASDEX upgrade [11]. A possible explanation for the rapid rotation is the role of neutrals [12] which are not included in standard neoclassical calculations.

References

[1] B.A. Grierson, et al., Rev. Sci. Instrum. 83, 10D529(6) (2012).
[2] S.R. Haskey, et al., Rev. Sci. Instrum. 89, 10D110 (2018).
[3] C. Chrystal, et al., Rev. Sci. Instrum. 87, 11E512 (2016).
[4] A. Blom and C. Jupén, Plasma Phys. Control. Fusion 44, 1229 (2002).
[5] S.R. Haskey, et al., Plasma Phys. Control. Fusion 60, 105001 (2018).
[6] D.J. Battaglia, et al., Plasma Phys. Control. Fusion 58, 085009 (2016).
[7] J.D. Callen, et al., Nucl. Fusion 50, 064004 (2010).
[8] W.M. Stacey, et al., Phys. Plasmas 14, 012501 (2007).
[9] E. Viezzer, et al., Nucl. Fusion 57, 022020 (2017).
[10] J. Kim, et al., Phys. Rev. Lett. 72, 2199 (1994).
[11] E. Viezzer, et al., Nucl. Fusion 54, 12003 (2014).
[12] P. Monier-Garbet, et al., Nucl. Fusion 37, 403 (1997).

This material is based upon work supported by the U.S. Department of Energy, Office of Science, Office of Fusion Energy Sciences, using the DIII-D National Fusion Facility, a DOE Office of Science user facility, under Awards DE-AC02-09CH11466 and DE-FC02-04ER54698.